Progress In Electromagnetics Research C, Vol. 107, 143–156, 2021

Fractal Minkowski-Shaped Resonator for Noninvasive Biomedical Measurements: Blood Glucose Test

Sarah M. Obaid[1, 2], Taha A. Elwi[2, *], and Muhammad Ilyas[1]

Abstract—This work presents a noninvasive measurement technique to detect the blood glucose level for diabetic individuals using a fractal microwave resonator printed on an FR-4 substrate. The proposed fractal is based on the 1st order of Minkowski open loops (MOL) coupled with an open-stub transmission line (OSTL) to increase the resonator selectivity at 2.45 GHz. Moreover, an air gap in the middle path of the OSTL is filled with multi wall carbon nanotubes patch (CNT) to increase the field fringing at a specific region. The proposed resonator is designed numerically with CST Microwave Studio. The size limitations for biomedical devices are considered to account for wearable applications. Later, an analytical study is presented on the proposed resonator sensitivity. The detection technique is based on the resonant frequency tuning, bandwidth variation, impedance matching change, and phase displacement for the S-parameters in the S_{11} and S_{12} spectra. The sample under test is mounted on a CNT patch of the OSTL which employs the characterization of the specimen. The proposed design idea could be generalized for a wide variety of biomedical detection liquids.

1. INTRODUCTION

In microwave ranges, sensing technologies based on materials dielectric and magnetic properties variation are still very promising candidates for many fields including biomedical applications [1]. Microwave measurements are very preferable in biomedical characterizations due to the ability of microwave radiations for penetrating noninvasively with good depth inside nonconductive materials [2]. Therefore, the material permittivity (ε) and permeability (μ) are important parameters for materials skin depth and attenuations [3]. In the last few years, many researchers applied planar microwave resonators with various applications. For example, in [4], the use of microstrip patch resonator based copper nano wires was for gas detection. The use of a composite left/right hand metamaterial patch antenna for water pollution detection was presented in [5]. The authors in [6] and [7] applied a microstrip line tee resonator for different constitutive parameters measurements. In [8], a microstrip transmission line was used for moisture level detection in oil products. In more relative studies for this work, the authors in [9] applied their study for characterizing samples of organic tissue and bio-microfluidics. However, diabetes represents one of the largest health concerns to the current century [10], where 17% of the world population is affected. Therefore, the work in many researches applied to monitor the blood glucose in real time process use microwave sensors. For example, coplanar waveguide sensor integrated with microfluidic system in [11], a spiral-shaped microstrip transmission line sensor [12], microstrip patch/slot antenna-based sensor [13], and millimeter-wave waveguide transmission measurement system [14] were proposed for glucose level measurements. The reported results out of such researches showed that the complex value of ε could be changed with the blood glucose concentration [15]. Therefore, a study

Received 26 July 2020, Accepted 20 November 2020, Scheduled 7 December 2020
* Corresponding author: Taha Ahmed Elwi (taelwi82@gmail.com).
[1] Electrical and Computer Engineering, Altinbas University, Turkey. [2] Department of Communication Engineering, Al-Ma'moon University College, Baghdad, Iraq.

in [16] proposed a microwave sensor prototype for monitoring the effective fluctuation in the blood glucose level in a laboratory environment.

Recently, many microwave devices relevant to printed circuit technology are advanced using metamaterial inclusions including microwave sensors. As developed in [17], a microwave sensor based on ring resonators was prepared to determine the dielectric constant of various materials. Split rings resonators (SRR) were introduced to the microwave resonator to realize a miniaturized structure for material constitutive parameters characterizations [18]. Nondestructive sensors were discussed in [19] and [20] based on SRR for low and high material losses measurements. In all previous studies, the effect of resonator geometry on the field distribution around the resonator and into the tissues was not discussed except in [21, 22] but with minimal justifications and details. Moreover, the use of artificial intelligent algorithms is still very limited in former characterization methods that are related to such research.

In the present work, a new resonator is based on four MOL unit cells coupled to OSTL with the CNT patch for blood glucose characterizations of diabetic people. The structure is printed on an FR4 to realize a frequency resonance at 2.45 GHz. A circuit model is derived to characterize the proposed sensor, and two numerical software packages are invoked for validation of the proposed design based on CST and HFSS algorithms. After finalizing the proposed sensor design, the sensitivity analysis is performed by invoking 15 blood samples. The procedure of sensing is developed based on a K-nearest neighbor (KNN) algorithm to quantize the glucose level. In Section 2, the resonator design is presented. The fabrication process and measurement validation are presented in Section 3. The sensing analysis and discussion are explored in Section 4. The paper is concluded in Section 5.

2. MICROWAVE RESONATOR DESIGN AND ANALYSIS

The proposed resonator in Fig. 1(a) is based on four Minkowski open loops, and each one of them performs a single MTM inclusion. Therefore, the relative constitutive parameters in terms of relative permittivity (ε_r) and permeability (μ_r) are retrieved to evaluate the effects of the inherent losses. Nevertheless, the reason of invoking the MTM is to support the backward wave propagation [22], which in turn realizes an excellent reduction factor with high selectivity performance. In Fig. 1, the proposed structure is presented with the relative equivalent circuit that will be used later for the theoretical analysis. As mentioned later, the proposed resonator consists of four MOL coupled with OSTL. The proposed resonator is structured to provide maximum fringing at the CNT patch in the OSTL. The individual MTM unit cell is constructed as a Minkowski loop with an effective length (L_n) to provide a resonant frequency (f_r). The loop length can be determined as:

$$L_n = (4 \times l - D)\left(\frac{27.4058 + n}{18.35}\right)^n \tag{1}$$

This can be used to calculate f_r as:

$$f_r = \frac{c}{1.617\left(\frac{7.7 - n}{7.6}\right)^n L_n \sqrt{\varepsilon_r}} \tag{2}$$

where l is the side length of the Minkowski loop, n the harmonic generation mode number, c the speed of light, and D the CNT patch dimension. It is important to mention that the proposed fractal is designed to fit a maximum current path within a limited area. Moreover, the trace width is minimized to 0.25 mm to avoid any radiation leakage at resonance [4] except from the CNT patch.

The array structure is mounted on an FR-4 substrate of 2 mm thickness with a ground plane on the back panel and $\varepsilon_r = 4.5 \pm j0.0019$. As mentioned later, MOL unit cells are coupled to an open stub transmission with the CNT patch for testing samples. The performance of the proposed resonator is studied as follows.

2.1. MOL Characterizations

The proposed unit cell is characterized theoretically to evaluate the S-parameters in terms of S_{11} and S_{12} spectra. Based on the equivalent circuit in Fig. 1(a), MOL unit cell equivalent circuit elements in

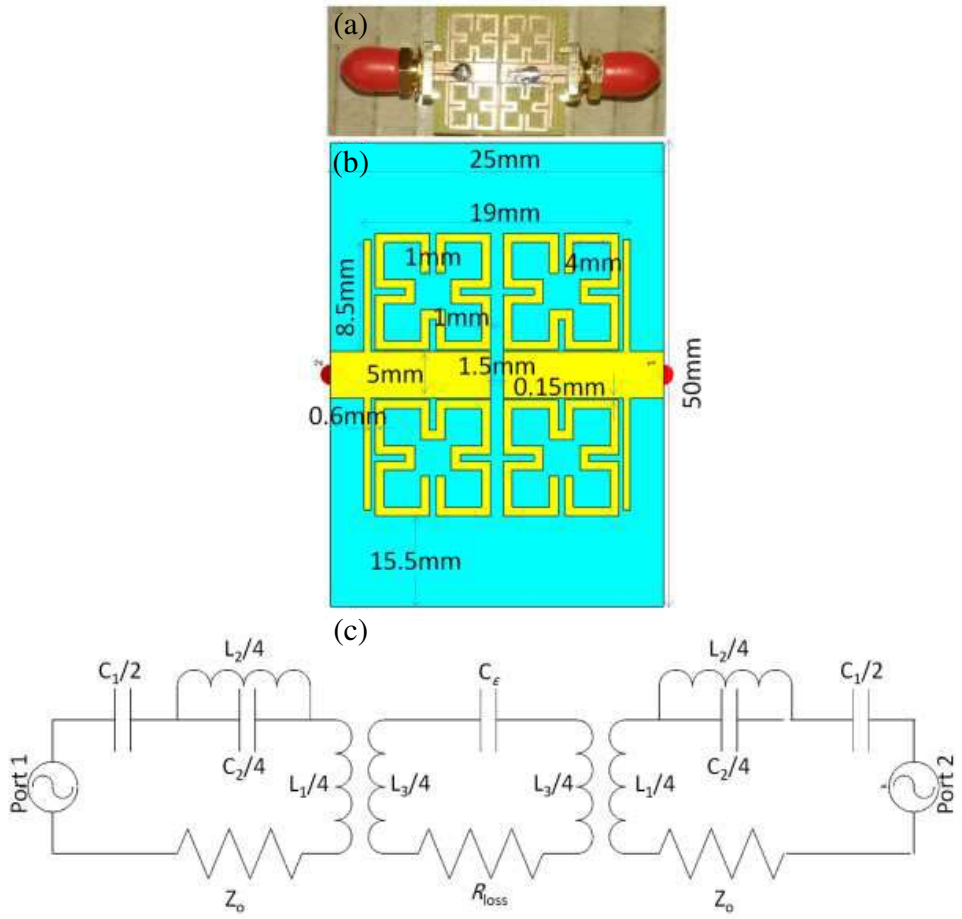

Figure 1. Microwave resonator layout: (a) geometrical details and (b) equivalent circuit diagram.

terms of LC branch can be evaluated from Richards frequency transformation method [2] by assuming $\gamma_o = 50$ with FBW $= 0.385$. Therefore, L_s, L_p, C_p, L_{s1}, and C_s are described by the following equations:

$$C_p = \left(\frac{1}{\text{FBW}\omega_0\Omega_c}\right)\frac{1}{\gamma_0 g} \tag{3}$$

$$L_p = \frac{1}{(\omega_0^2 C_p)} \tag{4}$$

$$C_s = \left(\frac{\Omega_c \text{FBW}}{\omega_0}\right)\frac{g}{\gamma_0} \tag{5}$$

$$L_{s1} = \frac{1}{(\omega_0^2 C_s)} \tag{6}$$

Next, the electromagnetic band gap of the proposed sensor is evaluated at the first Brillion zone as depicted in Fig. 2. It is found that the proposed unit cell possesses a band gap between 2.4 GHz and 2.55 GHz at normal incidence. Therefore, it is an excellent candidate to achieve a unit cell array for preventing the radiation leakage at 2.45 GHz.

2.2. OSTL Characterizations

Now, an optimization study is conducted based on circuit analysis to reach the required criteria at 2.45 GHz. The resulting lumped element values from this study are listed in Table 1. Nevertheless, it

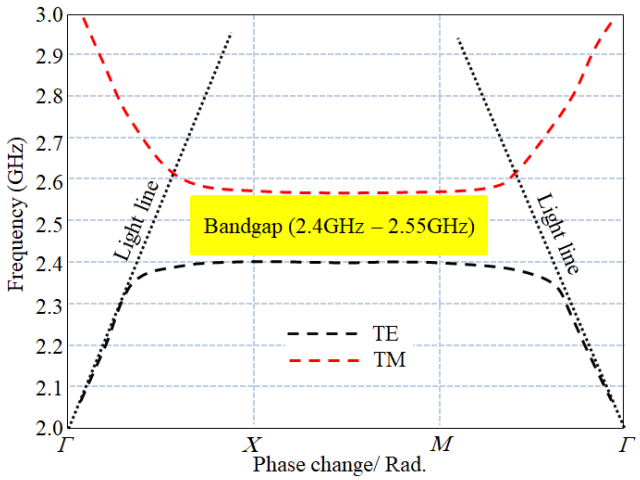

Figure 2. Dispassion diagram at the FBZ for the proposed MOL unit cell.

is found in the optimization process that there is a significant effect of C_{gap} on the frequency resonance as well as the matching impedance magnitude; however, the bandwidth is found to be insignificantly affected as seen in Fig. 3.

From the results in Fig. 3, the authors decided to derive relative impedance matching and the frequency resonance change with respect to C_{gap} and R_{gap}. Based on the circuit analysis in Fig. 1(b), the total impedance, Γ and $\Delta\omega_o$ are expressed as follows:

$$|\Gamma| = \sqrt{\frac{\left[(3R - Z_o)\,\omega L^2\right]^2 + \left[3\left(LR^2 - R\right)\right]^2}{\left[(3R + Z_o)\,\omega L^2\right]^2 + \left[3\left(LR^2 - R\right)\right]^2} \times \frac{\left[(Z_{eq} - 3R)\,\omega L^2\right]^2 + \left[3\left(LR^2 - R\right)\right]^2}{\left[(Z_{eq} + 3R)\,\omega L^2\right]^2 + \left[3\left(LR^2 - R\right)\right]^2}} \tag{7}$$

$$\Delta\omega_o = \sqrt{\frac{1}{L_p C_{\text{gap}}}} \tag{8}$$

Γ in Eq. (7) shows two possibilities for having zero reflection at lower and upper resonance frequencies at which the maximum transmission could occur. This provides a fact that at the CNT patch, the material characteristics of the sample under test would be the most effective reason for those two parameters to change as will be seen later.

Table 1. Values of equivalent circuit elements.

Elements	Value
L_1, L_2, L_3, L_4 (nH)	0.046
L_s (nH)	3.5
C_1, C_2, C_3, C_4 (pF)	95.2
C_{g1}, C_{g2}, C_{g3}, C_{g4} (pF)	0.52
L_p (nH)	1.8
C_p (pF)	2.443
L_{s1} (nH)	6.09
C_s (pF)	0.722
C_{gap}	0.15
R_{gap}	460

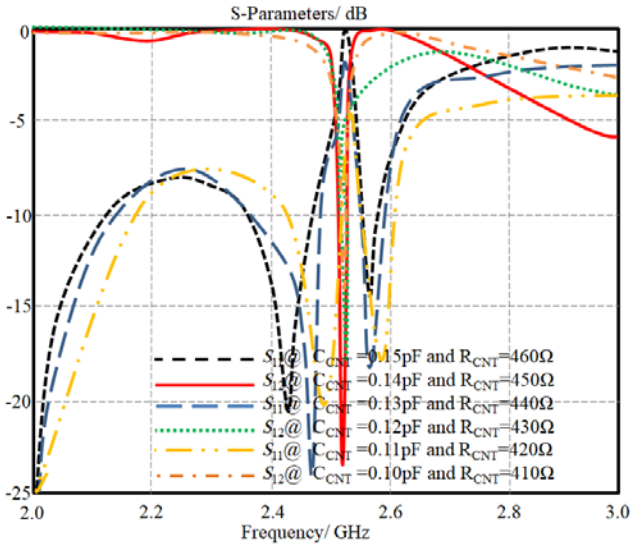

Figure 3. Effects C_{CNT} and R_{CNT} influence on the S-parameters.

2.3. Numerical Analysis

A parametric study, using CSTMWS, is conducted to realize the effect of the CNT patch area ($A = D^2$) in the OSTL on the S-parameters. The proposed resonator is excited with two discrete ports as presented in Fig. 1(a). A significant influence is found on the S_{11} spectra as seen in Fig. 4. As the parameter A increases, the zero at the upper side moves toward the stopband, but the zero at the lower side slightly moves away from the stopband without changing the resonance frequency. Nonetheless, increasing A more than 4 mm^2 dramatically affects the S_{12} spectra and frequency resonance. Therefore, it is found that the best performance of the proposed sensor occurs at 6 mm^2.

Now, the effects of changing the distance between MOL structures and the OSTL (S_{l1}) are investigated using a parametric study. The parametric study is conducted by changing the distance S_i from 1 mm to 3 mm with a step 1 mm and monitors the effects of that on the S-parameters. It is

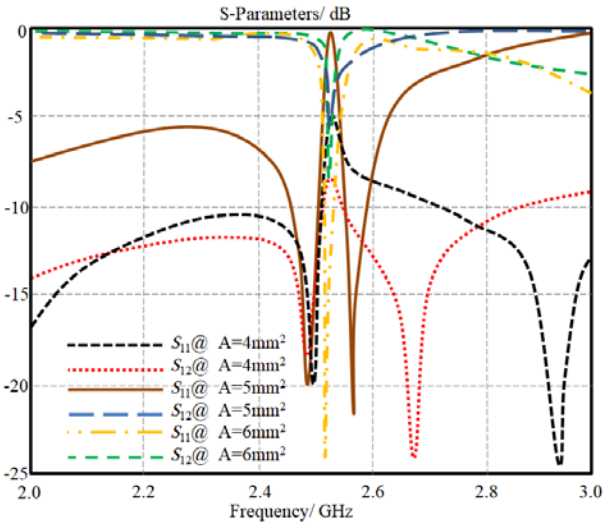

Figure 4. Effects of varying A on the S-parameters.

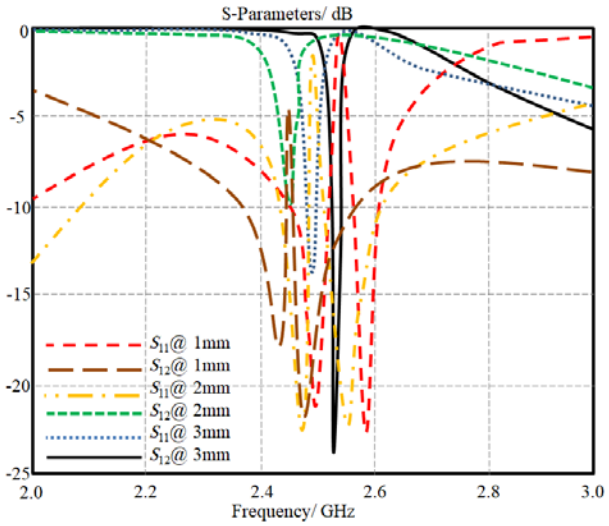

Figure 5. Effects of changing S_i distance on the S-parameters.

found that significant effects take place on the S_{11} bandwidth and S_{12} phase difference as seen in Fig. 5. This is attributed to the variation in the mutual capacitance and the fringing losses between the MOL and OSTL [12]. Therefore, it is found that such a change is an effective parameter on the proposed resonator. Hence, in the proposed sensor design, S_i value is fixed to 1 mm to have a frequency resonance located at 2.45 GHz in S_{11} magnitude spectra, while the phase difference for S_{12} spectra is considered as a reference level for measuring the samples later in this work. The magnitude of the S_{12} spectra is found to be less than -2 dB with two side zeros at 2.24 GHz and 2.6 GHz.

2.4. Theoretical Validation

To validate the achieved results, HFSS simulation software package was invoked before the fabrication process. For this, CST MWS simulation convergence test was considered to reach the optimal solution by discretizing the volume to 60, 60, and 53 in the x, y, and z axes. The performance of the proposed resonator is presented in Fig. 6 in terms of S-parameters in magnitude and phase spectra from both CST MWS and HFSS. It is observed that the obtained results from CST MWS and HFSS simulations excellently agree with each other. Finally, the numerical results from the used software packages are found to provide an acceptable agreement with the analytical results from the circuit theory analysis.

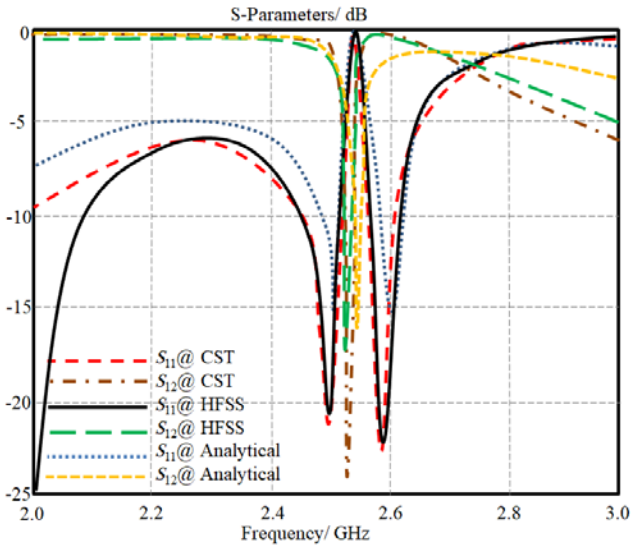

Figure 6. S-parameters validation for the proposed sensor.

3. SENSOR FABRICATION AND COLLECTED SAMPLES

The proposed sensor is fabricated with printed circuit board technology as seen in Fig. 7(a). The proposed sensor performance in terms of S-parameters in both magnitude and phase spectra are depicted in Fig. 7(b). The obtained results are compared to the simulated results from CST MWS for validation only. All measurements are obtained from Agilent 8722ES VNA after applying Short-Open-Load-Through (SOLT) Calibration process. Such calibration requires short, open, and 50 Ω load standards in the forward and reverse tracking plane in terms of error model. Therefore, a full one-port calibration and common through/reflection architecture on full two ports were performed. The same calibration process was performed based on the air reference with respect to the distilled water. This was conducted to avoid the bound water phenomena at the frequency range of interest between 2 GHz to 3 GHz at room temperature 25°C. All measurements were completed with 1600 points and -10 dBm input power. The measured S_{11} and S_{12} spectra of the unloaded resonator are presented Fig. 7(b). As observed from the results, excellent agreement is found with the numerical simulations in the specific frequency range.

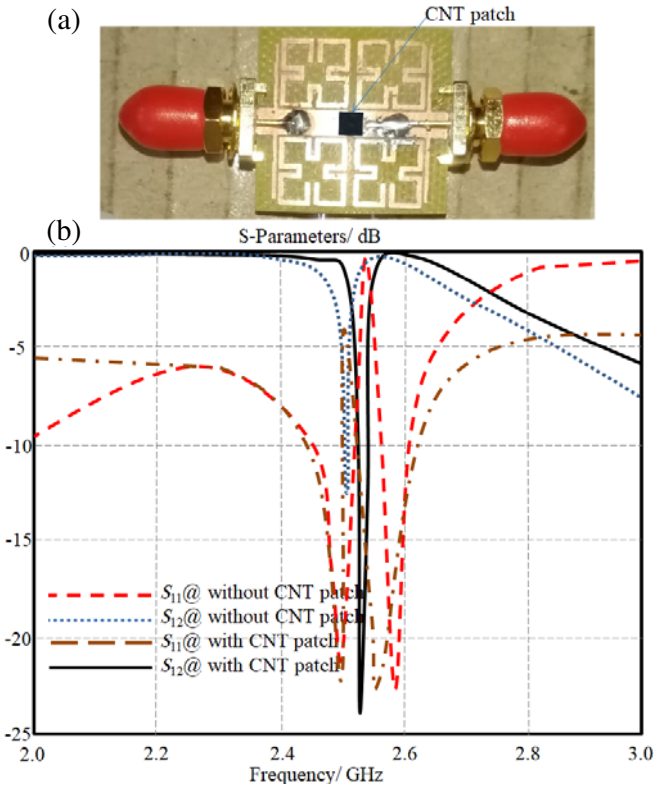

Figure 7. Experimental validation; (a) fabricated sensor and (b) measurements.

As a result of this comparison, the maximum resonance frequency shift is found from 2.4597 GHz to 2.457 GHz due to the plastic vessel introduction and soldering defects.

The proposed resonator in this section was constructed as a microwave sensor after introducing different blood samples through monitoring the S-parameters. Therefore, several blood samples were collected from different diabetic donors. In Table 2, we list the collected blood samples with the related details. The collected samples were considered with 15 different body mass indexes (BMI). The electromagnetic properties of each sample were measured using an open waveguide coaxial probe within the frequency range from 2 GHz up to 3 GHz [17].

4. SENSING MEASUREMENTS AND ANALYSIS

4.1. Sensing Process

The measured S-parameters of the proposed resonator with loads were obtained according to the listed samples in Table 2. The authors designed their resonator to ensure that the first resonance mode (f_o) was located around 2.45 GHz. Therefore, the fabricated resonator was used to retrieve ε_r and μ_r values from the S-parameters and compared to the listed values in Table 2. Consequently, the proposed samples were tested experimentally to evaluate the S-parameters using PNA8720 network analyzer. The resonant frequencies of S_{12} spectra of the proposed resonators without loading the proposed samples were considered as the reference resonances. Then, after loading the resonators with the listed samples in Table 2, the measured S_{12} spectra are presented in Fig. 8. The obtained S_{12} results were classified to three different groups as seen in Fig. 8. The classification is done according to the frequency resonance shift with respect to the original resonator response before loading the blood samples. Therefore, group_1 represents the samples that show insignificant change in the frequency resonance while the matching impedance is degraded with significant quality factor bandwidth. Group_2 is considered for the samples shifted up frequency resonance with insignificant matching impedance change and bandwidth

Table 2. Considered blood samples complex ε_r.

Case number	BMI	Age/year	Sex	Glucose level	ε_r'	ε_r''
1	19.1	7	F	102	72.2	0.106
				200	74.7	0.115
				156	73.9	0.111
2	24.9	51	F	111	72.8	0.109
				123	72.3	0.112
				201	75.3	0.115
3	21.4	70	M	300	77.2	0.121
				125	72.9	0.111
				245	76.3	0.156
4	28.1	45	M	301	76.9	0.116
				359	78.1	0.182
				277	78.4	0.174
5	26.7	56	M	231	74.5	0.123
				93	72.1	0.193
				108	72.4	0.191
6	32.1	35	F	122	73.1	0.103
				133	73.1	0.109
				143	73.9	0.108
7	33.5	43	F	185	74.1	0.122
				164	73.9	0.133
				166	72.4	0.124
8	29.8	42	F	101	73.1	0.091
				91	72.9	0.094
				98	73.0	0.092
9	23.4	49	F	144	74.1	0.091
				187	77.8	0.098
				145	77.4	0.092
10	32.6	37	M	190	76.3	0.109
				123	75.6	0.106
				144	76.1	0.110
11	36.1	72	M	102	72.4	0.111
				300	77.3	0.110
				340	77.9	0.113
12	34.6	67	M	390	77.8	0.189
				331	77.3	0.188
				301	77.0	0.177
13	21.4	63	M	210	74.9	0.109
				243	75.2	0.101
				226	75.1	0.105
14	22.5	68	M	189	74.2	0.195
				130	73.4	0.196
				210	74.4	0.179
15	23.8	54	M	221	75.3	0.109
				289	75.9	0.110
				234	75.2	0.112

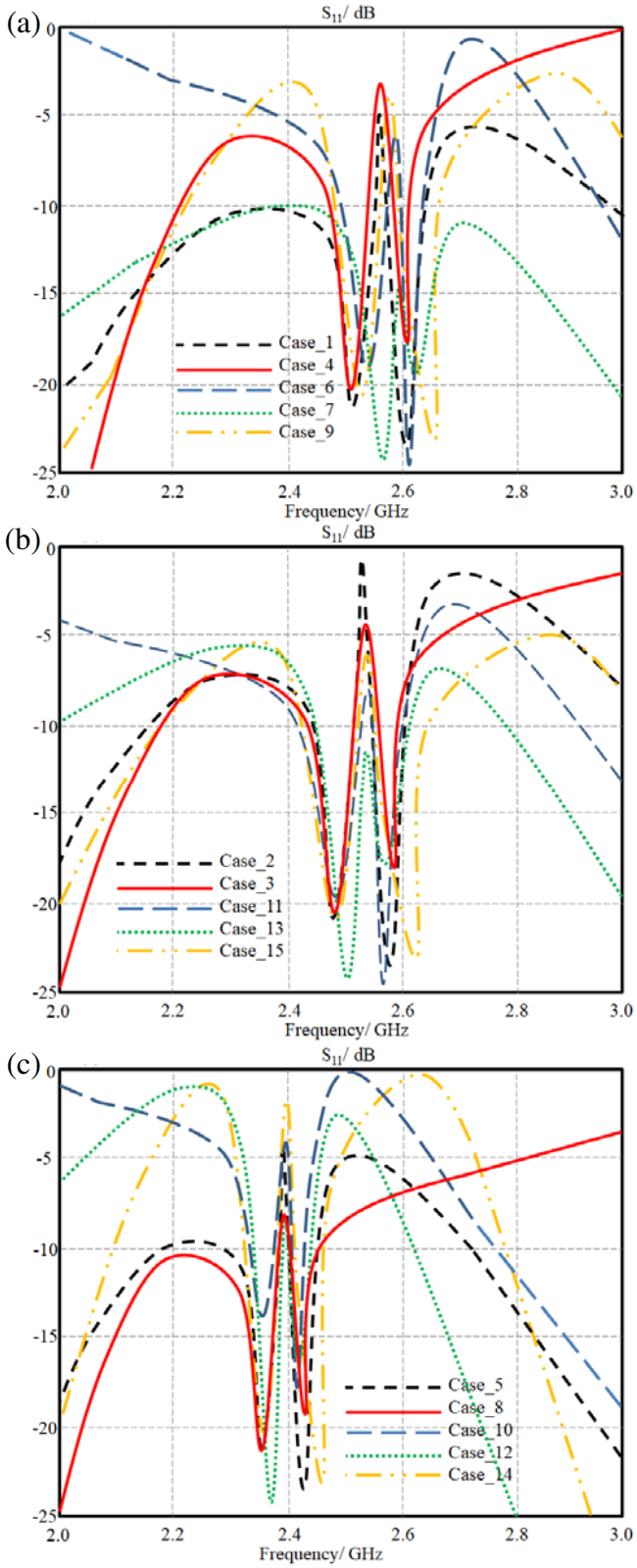

Figure 8. Measured S_{12} spectra of the proposed samples in comparison to the used T-resonators response; (a) for group_1, (b) for group_2, and (c) for group_3.

change. And group_3 is for the samples with lag frequency resonance shift and a dramatic change in the bandwidth. In the sense of that, the authors identify the best samples for the blood glucose classification minimum sensitivity errors as will be seen later.

From Fig. 8, it can be seen that the fundamental frequency resonance (f_o) of the proposed resonator is 2.45 GHΩz. After calcification, it is observed in Fig. 8(b) that f_o shows no significant changes in between the introduced blood samples from group_1; however, the quality factor is affected. It is observed in Fig. 8(b) by introducing the samples of group_2 that f_o is mostly shifted with increasing the glucose increase. On the other hand, the frequency is shifted back to 0.1 GHz, after introducing the samples of group three to the proposed resonator as seen in Fig. 8(c). Therefore, the variation in the frequency resonances at different mode numbers (N) from the resonator (f_{Rn}) with respect to the nearest neighbor mode in the relative sample under test (f_{sn}) is evaluated from Eq. (1):

$$\Delta f_n = \frac{\sqrt{\sum_{i=1}^{N} (f_{Rn} - f_{sn})^2}}{M} \tag{9}$$

where M is the number of measurements for each case and in our study is 5 samples for each case in each group. It should be noted that the calculated values differences (Δf_n) are computed from S_{12} spectra for each group as shown in Fig. 9. Later, the variations in the magnitude of S_{12} spectra (ΔS_{12}) with samples introduction are evaluated. Therefore, the average differences in the proposed resonator S_{12} magnitude (S_{12Rn}) with respect to S_{12} after sample introduction (S_{12s}) at each mode are calculated according to the following:

$$\Delta S_{12n} = \frac{\sqrt{\sum_{i=1}^{N} (S_{12Rn} - S_{12sn})^2}}{M} \tag{10}$$

This is considered in our calculation to evaluate the effects of material losses that are usually present the imaginary parts of ε_r and μ_r.

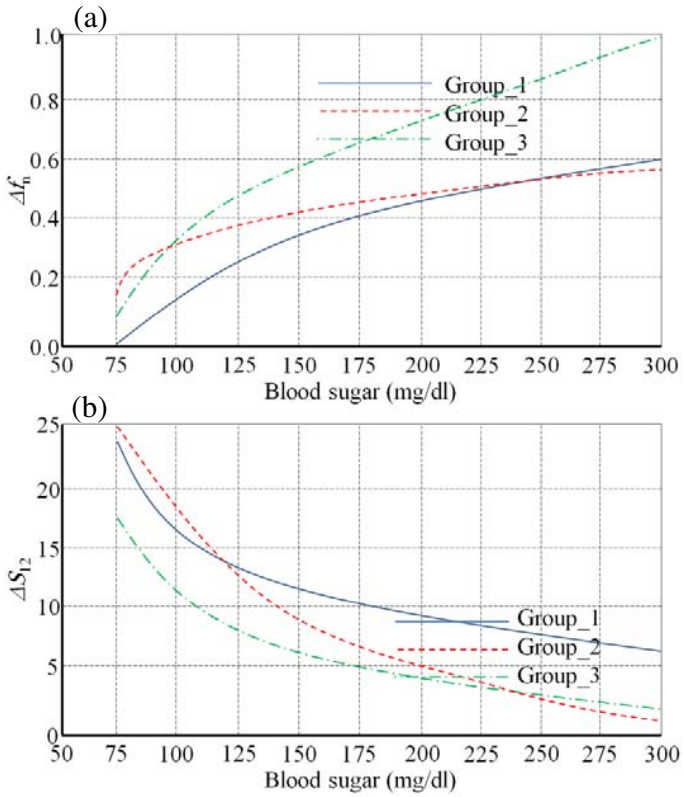

Figure 9. Average differences at different blood sugar levels for each group from S_{12} spectra; (a) frequency resonance variation and (b) S_{12} magnitude variation.

In general, from Fig. 9(a), the main variation in Δf_n can be noticed in group_2 and group_3 which is negative with the increase of mode number. However, the variation in group_1 is found almost insignificant with a constant slope from the resonator. Likewise, the relative changes in ΔS_{12} increase with the increase of mode number for group_2 and group_3 as seen in Fig. 2(b), while the changes in ΔS_{12} for group_1 are found almost constant. On the other hand, the guide wavelength λ_g related to the length of the stub length (L) of the T-resonator at the resonance mode that can be calculated as:

$$L + \Delta L = \frac{[2\,(N-1)+1]\,\lambda_g}{4} \tag{11}$$

where

$$\lambda_g = \frac{c}{f_{rn}\sqrt{\varepsilon_e}} \tag{12}$$

Therefore, by substituting Eq. (3) in Eq. (4), the resulting relation is given by:

$$\sqrt{\varepsilon_e} = \left[\frac{(2N-1)\,c}{4f_{rn}\,(L+\Delta L)}\right] \tag{13}$$

To compute the material losses, the quality factors (Q_L) are measured from the loaded resonator at 3 dB from the dip of S_{12sn} spectra at the resonance frequencies in comparison to the unloaded quality factor (Q_u) that is expressed as:

$$Q_u = \frac{Q_L}{\sqrt{1-(2)\,10^{((S12Rn-S_{12sn})/M10)}}} \tag{14}$$

Based on a neural network of K-Nearest Neighbor (KNN) algorithm that is adopted from [21] with input measurements, the relative values for ε_r and μ_r are retrieved. As explained in [22], the blood in general contains four materials (water, glucose, oil, and salt) mixed with different ratios. Therefore, to investigate the effects of each material ratio to the blood properties, the authors decided to find the first derivative of each curve in Fig. 9. Therefore, this requires calling the second polynomial curve fitting as an acceptable approximation process for retrieving the calibration function from the measured results in Fig. 9 as listed in Table 3. From the calculated results, we find that the models in group_3 are more promising than other groups, about 0.5% variation in the values of ΔS_{12}, which provides minimum attenuation effects. However, the maximum variation in that group in terms of Δf_n is found to be about 23%.

Table 3. Calibration equation and mixture percentage effects.

Case	Group Number	Calibration Equation	Mixture Percentage Effects
Our sensor	Group_1	$= 0.1M^2 - 0.04M + 0.22$	20%
	Group_2	$= 0.65M^2 - 0.21M + 0.1$	−16%
	Group_3	$= 0.8M^2 + 0.34M + 0.3$	−21%
	Group_1	$= 9.5M^2 + 4M + 9.5$	−21%
	Group_2	$= 2M^2 - 2M + 22$	50%
	Group_3	$= 3.5M^2 - 0.04M + 20$	0.5%
Traditional sensor	Group_1	$= 0.2M^2 - 0.3M + 0.7$	75%
	Group_2	$= .65M^2 + 0.21M + 0.3$	16%
	Group_3	$= 0.8M^2 + 0.37M + 0.6$	23%
	Group_1	$= 8.5M^2 + 4.6M + 10$	−27%
	Group_2	$= 2.4M^2 - 2M + 19$	42%
	Group_3	$= 6.5M^2 - 0.4M + 23$	3%

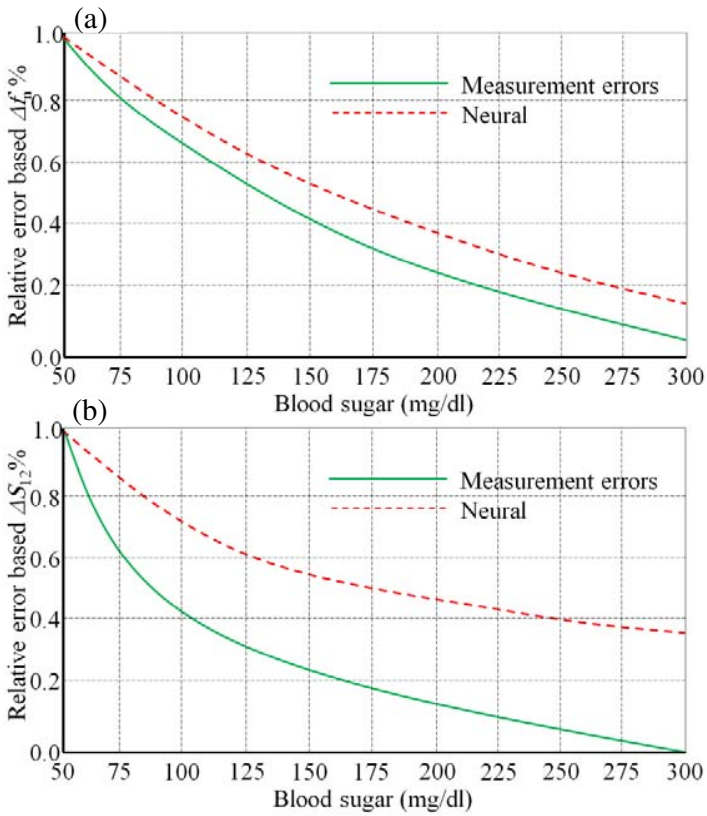

Figure 10. The sensitivity for the proposed measurements with respect to the traditional blood sugar measurements; (a) relative errors based on Δf_n and (b) relative errors based on ΔS_{12}.

From Table 3, the relative errors are calculated accumulatively between the estimated results based on the neural algorithm and the measurements for the blood glucose in the blood sample tests as shown in Fig. 10(a) based on the frequency shift, while the change in quality factor change is presented in Fig. 10(b).

5. CONCLUSION

The proposed sensor is presented for characterizing blood glucose of different samples. Therefore, the proposed sensor is designed based on a CNT patch to concentrate the electromagnetic fields to the material sample. In this case, the quality of the sample measurement would be enhanced significantly. A rectangular microwave resonator based on OSTL is coupled to four MOL unit cells. The resonator is proposed in this work to realize a highly selective structure with a narrow bandwidth for sensing operations. The measured performance of the fabricated prototype agreed reasonably with the theoretical results. It is found that the introduction of the CNT patch to the sensor design increased the radiated electric field leakage from the sensor center to suit the application of sensing, and the proposed sensor is a suitable choice for biomedical applications including measuring the blood glucose level. Therefore, fifteen cases are introduced to the proposed sensor to estimate the blood glucose level to end up with good agreement with the traditional commercial measurement process. All realized tests are included in a neural algorithm based KNN and curve fitting analysis. It is found that both conducted analyses are acceptable; however, the curve fitting analysis is more efficient. This is because the test date applied to the KNN algorithm was not sufficient to guarantee well predicated results. As a future work, the authors will add more training data to increase the accuracy of their process.

REFERENCES

1. Boybay, M. S. and O. M. Ramahi, "Material characterization using complementary split-ring resonators," *IEEE Trans. Instrum. Meas.*, Vol. 61, No. 11, 3039–3046, Nov. 2012.
2. Lee, C.-S. and C.-L. Yang, "Complementary split-ring resonators for measuring dielectric constants and loss tangents," *IEEE Microw. Wireless Compon. Lett.*, Vol. 24, No. 8, 563–565, Aug. 2014.
3. Yang, C.-L., C.-S. Lee, K.-W. Chen, and K.-Z. Chen, "Noncontact measurement of complex permittivity and thickness by using planar resonators," *IEEE Trans. Microw. Theory Techn.*, Vol. 64, No. 1, 247–257, Jan. 2016.
4. Naqui, J., C. Damm, A. Wiens, R. Jakoby, L. Su, J. Mata-Contreras, and F. Martín, "Transmission lines loaded with pairs of stepped impedance resonators: Modeling and application to differential permittivity measurements," *IEEE Trans. Microw. Theory Techn.*, Vol. 64, No. 11, 3864–3877, Oct. 4, 2016.
5. Puentes, M., C. Weiß, M. Schüßler, and R. Jakoby, "Sensor array based on split ring resonators for analysis of organic tissues," *IEEE MTT-S Int. Microw. Symp. Dig.*, 1–4, Baltimore, MD, USA, Jun. 2011.
6. Puentes, M., *Planar Metamaterial Based Microwave Sensor Arrays for Biomedical Analysis and Treatment*, Springer, Heidelberg, Germany, 2014.
7. Hardinata, S., F. Deshours, G. Alquié, H. Kokabi, and F. Koskas, "Miniaturization of microwave biosensor for non-invasive measurements of materials and biological tissues," *IPTEK Journal of Proceedings Series*, Vol. 1, 90–93, Jan. 29, 2018.
8. Chretiennot, T., D. Dubuc, and K. Grenier, "A microwave and microfluidic planar resonator for efficient and accurate complex permittivity characterization of aqueous solutions," *IEEE Trans. Microw. Theory Techn.*, Vol. 61, No. 2, 972–978, Feb. 2013.
9. Elwi, T. A. and W. J. Khudhayer, "A passive wireless gas sensor based on microstrip antenna with copper nanorods," *Progress In Electromagnetics Research B*, Vol. 55, 347–364, 2013.
10. Ebrahimi, A., W. Withayachumnankul, S. Al-Sarawi, and D. Abbott, "High-sensitivity metamaterial-inspired sensor for microfluidic dielectric characterization," *IEEE Sensors J.*, Vol. 14, No. 5, 1345–1351, May 2014.
11. Withayachumnankul, W., K. Jaruwongrungsee, A. Tuantranont, C. Fumeaux, and D. Abbott, "Metamaterial-based microfluidic sensor for dielectric characterization," *Sens. Actuators A: Phys.*, Vol. 189, 233–237, Jan. 2013.
12. Lee, H.-J. and J.-G. Yook, "Biosensing using split-ring resonators at microwave regime," *Appl. Phys. Lett.*, Vol. 92, No. 25, 254103, 2008.
13. Grenier, K., et al., "Integrated broadband microwave and microfluidic sensor dedicated to bioengineering," *IEEE Trans. Microw. Theory Techn.*, Vol. 57, No. 12, 3246–3253, Dec. 2009.
14. Chen, T., D. Dubuc, and K. Grenier, "Resonant-based microwave biosensor for physiological liquid identification," *Proc. Eur. Microw. Conf.*, 448–450, Amsterdam, The Netherland, Oct./Nov. 2012.
15. Chretiennot, T., D. Dubuc, and K. Grenier, "Optimized electromagnetic interaction microwave resonator/microfluidic channel for enhanced liquid bio-sensor," *Proc. Eur. Microw. Conf.*, 464–467, Nuremberg, Germany, Oct. 2013.
16. Chretiennot, T., D. Dubuc, and K. Grenier, "Double stub resonant biosensor for glucose concentrations quantification of multiple aqueous solutions," *IEEE MTT-S Int. Microw. Symp. Dig.*, 1–4, Tampa, FL, USA, Jun. 2014.
17. Ekmekci, E. and G. Turhan-Sayan, "Multi-functional metamaterial sensor based on a broad-side coupled SRR topology with a multi-layer substrate," *Appl. Phys. A, Solids Surf.*, Vol. 110, No. 1, 189–197, Jan. 2013.
18. Wongkasem, N. and M. Ruiz, "Multi-negative index band metamaterial-inspired microfluidic sensors," *Progress In Electromagnetics Research C*, Vol. 94, 29–41, 2019.
19. Damm, C., M. Schüßler, M. Puentes, H. Maune, M. Maasch, and R. Jakoby, "Artificial transmission lines for high sensitive microwave sensors," *Proc. IEEE Sensors Conf.*, 755–758, Christchurch, New Zealand, Oct. 2009.

20. Damm, C., *Artificial Transmission Line Structures for Tunable Microwave Components and Microwave Sensors*, Shaker Verlag, Aachen, Germany, 2011.
21. Turgul, V. and I. Kale, "Permittivity extraction of glucose solutions through artificial neural networks and non-invasive microwave glucose sensing," *Sens. Actuators A: Phys.*, Vol. 277, 65–72, 2018.
22. Turgul, V. and I. Kale, "Sensitivity of non-invasive RF/microwave glucose sensors and fundamental factors and challenges affecting measurement accuracy," *Proceedings of the 2018 IEEE International Instrumentation and Measurement Technology Conference (I2MTC)*, 1–5, Houston, TX, USA, May 14–17, 2018.